Usability of water surface reflectance for the determination of riverine dissolved methane during extreme flooding in northeastern Siberia

Tomoki Morozumi*[a,b], Ryo Shingubara[a,j], Jun Murase[c], Shin Nagai[d,e], Hideki Kobayashi[e,d], Shinya Takano[a], Shunsuke Tei[b,f], Rong Fan[a,b], Trofim C. Maximov[g,h,], Atsuko Sugimoto[b,f,i]

[a]Graduate School of Environmental Science, Hokkaido University, N10W5 Sapporo, Hokkaido 060-0810, Japan

[b]Arctic Research Center, Hokkaido University, N21W11 Sapporo, Hokkaido 001-0021, Japan

[c]Graduate school of Bioagricultural Sciences, Nagoya University, Furo-cho, Chikusa-ku, Nagoya 464-8601, Japan

[d]Research and Development Center for Global Change, Japan Agency for Marine-Earth Science and Technology, 3173-25 Showa-machi, Kanazawa-ku, Yokohama, Kanagawa 236-0001, Japan

[e]Institute of Arctic Climate and Environment Research, Japan Agency for Marine-Earth Science and Technology, 3173-25 Showa-machi, Kanazawa-ku, Yokohama, Kanagawa 236-0001, Japan

[f]Faculty of Environmental Earth Science, Hokkaido University, N10W5 Sapporo, Hokkaido 060-0810, Japan

[g]Institute for Biological Problems of Cryolithozone, Siberian branch of Russian academy of Sciences, 41 Lenin Ave., Yakutsk, 677980, Russia

[h]North-Eastern Federal University, 677000 Yakutsk, Russia

[i]Global Station for Arctic Research, Global Institution for Collaborative Research and Education, Hokkaido University, N21W11 Sapporo, Hokkaido 001-0021, Japan

Present address:

[j]Graduate school of Environmental Studies, Nagoya University, Furo-cho, Chikusa-ku, Nagoya 464-8601, Japan

*Corresponding Author: Tomoki Morozumi, Graduate school of Environmental Science, Hokkaido University, N10W5 Sapporo, Hokkaido 060-0810, Japan, Tel.: +81(11)706-2233, Fax: +81(11)706-4867, E-mail: both-horns@ees.hokudai.ac.jp

Highlights:

- Dissolved methane in Arctic freshwater is an important atmospheric methane source
- Surface reflectance (water color) can serve as a proxy for methane concentration
- Analysis of Siberian floodwater samples and satellite data confirm this method

ABSTRACT

An extreme flooding event occurred from June to July 2017 in the Indigirka River lowland of northeastern Siberia. We used Landsat 8 satellite surface reflectance data to detect the flood inundation area and extract water color for delineating different water sources. We also took direct samples of dissolved methane concentrations in the river water. Relatively high concentrations of dissolved methane (0.7–1.1 μmol l^{-1}, or μM) were observed in four tributary areas in 2017 during the flood's recession, while the values remained low in the main channel (0.2–0.3 μM). In contrast, the concentrations of dissolved methane were low in both the main channel and tributaries during the non-flood period of 2016 (0.1–0.2 μM). We then used 2017 satellite reflectance data with an empirical model to estimate the spatial differences of dissolved methane concentration for water sources contributing to the methane-poor main channel and methane-rich tributaries and applied the results to the calculation of riverine methane in the study region (approx. 200 × 300 km). This approach to estimating dissolved methane concentrations using satellite reflectance can provide a new tool for environmental monitoring of flood events in remote areas.

***Keywords*:** Flooding, Dissolved methane concentration, Arctic, Landsat 8

1. Introduction

Dissolved methane (CH_4) is an important factor in aquatic biogeochemical cycles; river water is usually oversaturated with methane, such that the riverine flux contributes to increases in atmospheric methane (Campeau and del Giorgio, 2014; Sawakuchi et al., 2014; Striegl et al., 2012). Additionally, highly saturated dissolved methane is transported to the ocean, where it can be an important methane source in high-latitude coastal areas (Shakhova et al., 2007). Dissolved methane is produced by the decomposition of organic carbon under anoxic conditions and consumed by microbial oxidation, which is activated when the oxygen concentration of river water increases (Stanley et al., 2016). The riverine production/consumption balance is controlled by landscape patterns of river channels connected to streams, lakes, wetlands and ponds that are related to basal sediment compositions (Crawford et al., 2017).

Dissolved methane concentrations can have large spatial and temporal variations including the seasonal dynamics observed in rivers and other terrestrial water bodies. In low-latitude regions such as the Amazon River Basin, the dissolved methane concentration has been reported to rise during periods of low or declining water levels, especially in tributaries (Barbosa et al., 2016). In high-latitude regions, dissolved methane can be enriched owing to seasonal accumulations of methane under lake ice (Langer et al., 2015), contributing to high methane emissions when the ice breaks up in spring (Karlsson et al., 2013). Changing concentrations of dissolved methane have also been observed in a Finnish river during snowmelt (Dyson et al., 2011). Therefore, seasonal changes in high-latitude water tables and river discharges can affect dissolved riverine methane concentrations and fluxes.

Such dissolved methane fluxes can be studied using satellite remote sensing to provide a broader spatial coverage of the inundation area (Rokni et al., 2014) and to determine water color from turbidity using optical reflectance from suspended sediment on the surface (Mertes et al., 1993, Volpe et al., 2011, Ward et al., 2013). Xiao et al. (2017) introduced an empirical stepwise regression for methane flux determination in shallow lakes using observed water clarity, dissolved oxygen data, and the satellite-derived normalized difference vegetation index (NDVI).

In early summer (June–July) 2017, major flooding in the Yana-Indigirka lowland of northeastern Siberia covered a large region with water. Surface water derived from snow and/or ice melt (including lake water) was likely mixed with river water during the flood. We hypothesized that different water sources with distinct levels of dissolved methane and suspended sediments (represented by water color) were mixed during this event, and that their spatial distributions could be distinguished under flood conditions in the main channel and tributaries.

Thus, we collected in-situ concentrations of riverine dissolved methane and surface reflectance satellite data during the summers of 2016 and 2017. Using the 2017 data during the flood period, we also modeled the dissolved methane concentration using water reflectance and estimated the river's methane flux for both years. Our results demonstrate a new approach to estimating dissolved methane using water color reflectance data and offer new insights into methane emissions during an extreme flooding event in northeastern Siberia.

2. Methods and Data

2.1. Study location and observation methods

We focused on the lower reaches of the Indigirka River and its tributaries near Chokurdakh in northeastern Siberia (Figure 1). The landscape consisted of a taiga-tundra boundary ecosystem with many lakes, ponds, and wetlands among shrubland and sparse stands of larch trees. The area's climate is extremely cold with a mean annual air temperature of −13.9°C (measured during 1950–2008; Liang et al., 2014; Yabuki et al., 2011). Water level was recorded every 1–3 days from mid-July to early August during 2015–2017 at two sites, Chokurdakh (70.62° N, 147.89° E) and Kodac (70.56° N, 148.15° E); these sites were also used by previous studies (Iwanhana et al., 2014; Liang et al., 2014; Figure 1b). We recorded river levels directly by measuring the vertical distance from a tagged tree to the river surface, because there are no river gauging stations close to the field site. In addition, we observed river flooding indirectly using time-lapse cameras (Garden Watch Cam, Brinno, USA) and using satellite imagery (see section 2.3).

2.2. In situ dissolved methane measurements

We collected river surface water samples (upper 10 cm) from a motorboat on 8 and 25 July 2016 (6 samples for each) and 28 July and 2 August 2017 (5 samples for each) using a 60-ml plastic syringe with a three-way stopcock (Figures 1b, 2). Samples of river surface water were obtained from three areas of the Indigirka river system: the main channel, substream (west area) and tributaries (east narrow channels in the eastern area; Figure 1b). Methane free headspace gas and river water samples was mixed in the plastic syringe for 1 minute. After a leave for 5 minutes , methane was extracted to the head space gas under equilibrium at room temperature and pressure. Ultra-high purity N_2 gas was used as the headspace gas (45 ml of water and 15 ml of N_2 in a 1:3 ratio) and headspace gas was transferred into a 10-ml vacuumed glass vial with a butyl rubber stopper and was brought to the laboratory at Hokkaido University, Japan. Methane concentration in the sample gas was measured using gas chromatography with a flame-ionization detector (GC-FID; HP6890, Hewlett Packard, USA). The detection limit in the gas chromatography (GC) analysis was less than 0.07 µM and the reproducibility of the analysis was less than 0.16 ppm. Finally, the initial concentration of dissolved methane was calculated with a Bunsen coefficient obtained by Yamamoto, 1976. Concentrations in µmol l^{-1} were recorded in units of µM (micro molar). We also used data for dissolved methane concentrations from 13 samples taken at three points within a lake near a tributary (Figure 1b) on the 20, 25, and 27 July 2013 (non-flood), using similar methods (Shingubara et al., 2016). Additionally, four ambient air samples were collected at wetlands near the Indigirka's main channel on 10, 19, 20, 24 and 27 July 2016 and 30 July 2017, for use in flux calculations (section 2.5). The measured values were statistically analyzed by t-test using p value notation.

2.3. Flooding and water color detection using satellite imagery

We acquired Landsat8 Operational Land Imager (OLI) surface reflectance images (30 m resolution) of the study area for 29 June, 29 July, and 7 August 2016 and 11 and 27 July 2017 (USGS/NASA; Figure 2, Table 1) and observed the water color. The 11 July 2017 image (Figure 1d) was used for detection of flooded areas and for water color analysis when the water was at its highest; the 27 July 2017 image (Figure 1d) represented a ~60% retreat of floodwater compared with the peak flood height on 11 July.

Satellite image analysis and classification were conducted using the ENVI v5.1 software (Exilis Visual Information Solutions, Broomfield, CO USA), and spatial patterns were analyzed with ArcGIS v10.2 (Environmental Systems Research Institute, Redlands, CA USA). Water extent (and thus flooding) was defined by normalized difference water index (NDWI; McFeeters, 1996) values exceeding a threshold of 0.05 value; NDWI is defined as:

$$\text{NDWI} = (\text{Green} - \text{NIR}) / (\text{Green} + \text{NIR}), \quad (1)$$

where Green is Band 3 (533–590 nm) and NIR is Band 5 (851–879 nm). Water surface reflectance (water color) data were acquired using the nearest 4 pixels, including at the sampling sites for dissolved methane (within 1–5 days before sampling). Pixels were carefully selected from a homogenous water surface to avoid terrestrial pixels, shadow, breaking wave bubbles, glint, and other water color variations. Several indicators of water color were used, including reflectance on bands 1–7, NDWI, and the normalized difference vegetation index (NDVI):

$$NDVI = (NIR - Red) / (NIR + Red), \quad (2)$$

where Red is Band 4 (636–673 nm) and NIR is Band 5.

2.4. Empirical modeling of dissolved methane concentrations

To develop an empirical model for dissolved methane concentrations, we used the river surface reflectance as a proxy for the spatial distribution of the mixing processes between methane-rich and methane-poor water during flooding on 11 July 2017 (Figure 2). First, we applied multivariate correlation analysis and clustered samples by methane concentration and water color using the R software (R Core Team, 2013). A linear relationship between water color and methane concentration was assumed, and this linearity should be tested under various flooding condition in further research. Then, four groups among various methane concentrations (high-low) and water colors (clear-turbid) were distinguished as endmembers.

We used endmembers and a mixing model in a similar manner as to many other studies of stream water solute chemistry (e.g., James and Roulet, 2006; Neal et al., 2010). Our empirical mixing model was defined assuming main channel water (turbid) and tributary water (not turbid) as the endmembers:

$$\rho_{sample} = \rho_m \times F_m + \rho_t \times F_t, \quad (3)$$

$$C_{sample} = C_m \times F_m + C_t \times F_t, \text{ and} \quad (4)$$

$$F_m + F_t = 1, \quad (5)$$

where ρ_{sample}, ρ_m, and ρ_t are the reflectance of sampling points and endmembers in the main channel and tributary, respectively; F_m and $F_{t.}$ are the fractions of the main channel and tributary; and C_{sample}, C_m, and C_t are the dissolved methane concentrations of the sampling points, main channel, and tributary, respectively. The reflectance values were calculated in a scale factor of 0 to 10. The regression for reflectance and dissolved methane was given as:

$$C_{sample} = slope \times (\rho_{sample}) + intercept. \quad (6)$$

After obtaining predicted values for slope and intercept, we validated model performance using a subset of the observation data with intermediate reflectance and dissolved methane by clustering with the multivariate correlation analysis as described above. Correlation coefficient, root mean square error (RMSE), and Akaike Information Criteria (AIC) for the model were also used for evaluating the accuracy of the model.

2.5. Estimation of river flux

The methane flux (mg CH_4 m^{-2} d^{-1}) between the river surface and the atmosphere was calculated with a gas transfer velocity (k_{CH4}) using the difference between predicted concentrations in the river (C_w) and observed concentration in the atmosphere (C_a) in 2017 (Figure 2):

$$Flux = (C_w - C_a) \times k_{CH4} \ (mg\ CH_4\ m^{-2}\ d^{-1}). \quad (7)$$

Parameterization for the transfer velocity of methane was assumed by analogy to riverine CO_2 gas in boreal arctic zones as reported by Aufdenkampe et al. (2011):

$$k_{CH4} = k_{600}\ (Sc_{CH4}/400) \times 0.69\ (m\ d^{-1}), \quad (8)$$

where k_{600} is the CO_2 gas transfer velocity and $ScCH_4$ is the Schmidt number for methane given by a temperature dependence function (Wanninkhof, 1992). The Bunsen coefficient (Yamamoto, 1976) was then applied to estimate the saturation ratio of dissolved methane. The calculated flux values were the same range as the flux directly observed using a floating chamber at the site (0.5-3.4 mg m^{-2} d^{-1}; Morozumi et al., 2017).

2.6. Land cover analysis

We conducted land cover classification using Landsat multispectral data (bands 1–7) from 7 August 2016 (Table 1, Figure 2). Multiband images were classified by ISODATA unsupervised classification (ENVI), then mapped using vegetation types drawn from the high-resolution vegetation map produced using the supervised maximum likelihood method (Morozumi et al. 2016), which contains 8 types of vegetation classes, including tree, shrub, willow, and cotton-sedge. The land cover data obtained were used to consider methane sources because dissolved methane can be highly saturated in near-surface soil water in wetlands (Shingubara et al., 2016). Sedge wetland and aquatic lake margin areas up to 500 m from the river bank were selected as potential methane sources, and were delineated using the spatial multi-ring buffering tool in ArcGIS using 50 m intervals up to 200 m from the river and 100 m intervals 200–500 m from the river. Coverage proportions of methane source landscapes were then compared between the main channel and the tributaries.

3. Results

3.1. Dissolved methane concentrations of river water in 2016 and 2017

Large differences were detected in the methane concentrations of the main channel and tributaries between 2016 (normal year) and 2017 (flooding event). Dissolved methane concentrations of tributaries (0.7–1.1 µM) were significantly higher (p<0.005) than those of the main channel (0.2–0.4 µM) at the end of the extreme flooding event on 27 July and 2 Aug 2 2017 (Figure 3), while dissolved methane concentrations were low (0.1–0.2 µM) in both the main channel and tributaries on 8 July and 25 July 2016. Additionally, the dissolved methane concentrations of lake water were high (0.3–1.5 μM) in the summer of 2013 (Shingubara et al., 2016).

3.2. Water color in the flooding area

Using NDWI, extreme flooding water cover was detected across ~10,010 km^2 within a total area of ~59,830 km^2 on 11 July 2017. Physical observations showed that water levels were 2–3 m higher than in previous years. The time-lapse camera at the Kodac site captured flood conditions within forested land along a tributary from 11 June to 25 July, 2017.

Water surface reflectance values for both the main channel and tributaries were higher in 2016 (normal year) than in 2017 (flood year) for bands 3 and 4 (Figure S1). Tributary surface reflectance (mean and SD), which was expressed with a scale from 0 to 10, in 2017 for bands 3 and 4 were 0.137 ± 0.040 and 0.153 ± 0.053, respectively, lower than the main channel (0.287 ± 0.094 and 0.343 ± 0.101, respectively; $p < 0.001$). On the other hand, there was no statistically significant difference in 2016, although the average surface reflectance for the tributaries was lower than for the main channel.

3.3. Empirical end-member model for water color and dissolved methane concentrations

Dissolved methane concentrations were negatively correlated with band 4 (red, $R = -0.86$) and band 5 (NIR, $R = -0.87$) reflectance (Figure S2). We produced end-member models using these correlations. Before establishing the models, clustering analysis was used to determine the possible endmembers and outliers; the latter were removed from the model because of specific reflectances from tributaries close to lake outlets, as discussed in section 4.1. The clustering results produced four classes indicating (c1) high concentration and low reflectance, (c2) low concentration and high reflectance, (c3) intermediate, and (c4) high concentration and high NDVI and high NDWI (Figure S2); (c4) was considered an outlier. We also removed (c3) for use as evaluation data, as described in the methods.

Using the (c1) and (c2) data, end-member models with bands 4 and 5 were developed (Figure 4a). Methane predicted with the band 4 model was compared with the observed methane concentrations (Figure 4b; $R^2 = 0.94$, RMSE = 0.097, AIC = −9.44). Modeled concentrations of dissolved methane were mapped at a regional scale (~250 km; Figure 4c) and for local sampling areas (~50 km; Figure 4d). The main channel of the Indigirka River showed lower values of predicted methane concentrations, while the tributaries were relatively higher.

3.4. Regional river methane flux

The main channel (320 km^2) and tributaries (164 km^2) had average methane concentrations of 0.36 and 0.68 μM, respectively (Table 2), 187 and 351 times higher than water saturation at a temperature of 10 °C. Estimated average flux values were 5.6 and 16.5 mg CH_4 m^{-2} d^{-1} for the main channel and tributaries, respectively. Daily surface methane emissions from the total area of the main channel and tributaries were 1839 kg CH_4 d^{-1} (40.5% of the total river areas) and 2705 kg CH_4 d^{-1} (59.5%), respectively.

3.5. Land cover characterization

Land cover types were visually observed at each sampling point and checked against the classification (Figure 5). The distribution patterns of the lake-margin and sedge-wetland classes, considered to be the main sources of methane (van Huissteden et al., 2005; Shingubara et al., 2016), were different along the main channel and tributaries within the 500 m zone previously defined (Figure S3). The tributaries were surrounded by sedge-wetland and lake-margin (mostly

> 50%), whereas the main channel showed less sedge-wetland and more willow bushes, considered to have very low methane flux and concentrations (van Huissteden et al., 2005; Morozumi et al., 2016), along with a wider river channel. The ratios of sedge-wetland and lake-margin to total land cover were 25%–75% along the tributaries and 15%–40% along the main channel, whereas those of willow were 5%–13% along tributaries and 6%–20% along the main channel (Figure S3).

4. Interpretations and Discussions

4.1 Spatial variations in dissolved methane and water color

Our estimates of dissolved methane concentrations based on water color were higher in the tributaries than in the main channel in 2017 (Figure 4c, 4d) and surface water reflectance was negatively correlated with dissolved methane (Figure 4a). The main channel was turbid because of sediment transported from upstream areas with lower dissolved methane, whereas the tributaries were relatively clear with higher dissolved methane. In other words, dissolved methane was mostly sourced from tributaries within the Indigirka River lowlands, instead of upstream areas along the main channel from which most suspended sediments were sourced (Huh et al., 1998). On the other hand, in the summer of 2016, the dissolved methane concentrations in the tributaries were as low as in the main channel. Optical properties of tributaries' water can also be affected by dissolved organic matter, which is a potential substrate of methane, leaching from wetland soils, and has a dark color with light absorption (i.e., Brezonik et al., 2015), although these characteristics might be masked by the large variations of surface reflectance derived from light scattering by suspended sediments, in particular during 2017.

Dissolved methane concentrations sampled between 2016 and 2017 were similar in the main channel, whereas reflectance was different between the two years. Water color results indicated that turbidity in tributaries and the main channel were higher in 2016 than in 2017 for bands 3, 4, and 5 (Figure S1). The main channel is usually turbid during the spring snowmelt season owing to erosion in mountainous upstream regions, such that this turbid water mixes with clearer water in the lowlands. However, during the extreme flooding event in 2017, this turbid upstream water may have mixed with larger amounts of lowland water, causing the lower turbidity. In addition, a large amount of precipitation, and snowmelt water from thick snow cover in the lowlands, may also have contributed to the lower turbidity in 2017.

As noted in section 3.3, there was an outlying sample (c4) that contained a high concentration of dissolved methane (Figure 3) and showed relatively higher reflectance values along with high NDVI and NDWI (Figure S2). This sample was collected from a tributary close to the outlet of a lowland lake at a site surrounded by stands of willow and aquatic grasses; thus, there was the potential for aquatic plants to produce high NDVI. Xiao et al. (2017) reported that high NDVI and methane concentrations can be explained by *in-situ* methane production linked to the decomposition of aquatic plants and algae in subtropical lakes. As the sampling point for outlier (c4) in the tributary was close to the lake outlet, dissolved methane from the lake may have been high owing to the decomposition of organic matter.

4.2 Potential sources of dissolved methane in tributaries

During the extreme flooding event, there may have been two origins for the excess water: local snow melting under floodwater and water from the main channel. As the dissolved methane in the main channel was low, the source of dissolved methane in the tributaries must have been produced on the land, when the floodwater receded, and the tributary channels were re-established. There are usually several sources of methane on land, such as wetlands and lakes; during floods, vegetation such as trees and shrubs (which are usually methane sinks) might become sources owing to the anoxic condition of the soil. Any methane produced on the land can be carried away by the tributary. Compared with the 2017 flood, during the summer of 2016 the tributary water was poor in methane, owing to lower methane production and higher methane oxidation on the dry land (i.e., the normal condition).

Another possible reason for the higher methane concentrations in the tributaries might be the land cover. Higher ratios of sedge-wetland and lake-margin (> 50%) were observed close to the tributaries than along the main channel (Figure 5), which could have produced more methane (e.g., Billett and Harvey, 2013; Fernandez et al., 2016; Murase et al., 2003), whereas land cover close to the main channel was more commonly willow thickets on sand bars with only limited wetlands. The vegetation types close to the main channel are not typically considered methane sources (van Huissteden et al., 2005), so when flooding occurs, the vegetation along tributaries produces more methane than that along the main channel.

Finally, the relatively large amount of water in the main channel means that the low concentration of dissolved methane in the main channel is not strongly affected by the inflow of tributaries with higher concentrations.

4.3 Contributions of riverine methane emissions during extreme flooding on a regional scale

An extreme flooding event influenced an extensive region of river lowlands in eastern Siberia from June to July 2017. We reported that the dissolved methane concentrations along the Indigirka River and its tributaries (0.1–1.1 μM) were slightly higher than those previously reported at Lena river (0.01–0.7 μM), the adjacent catchment to our study location (Bussmann, 2013; Semiletov et al., 2011), and a small tributary of Yenisei in central Siberia (0.01-0.02 μM;

Morishita et al., 2014). The large temporal variations of dissolved methane concentration would cause the uncertainty in the regional estimate. However, the dissolved methane concentrations in this study are not extremely high compared with a middle Lena tributary (0.1-1.9 µM; Sawamoto et al., 2006), Yukon river main stem and tributaries (0.15–0.82 µM; Striegl et al., 2012), and even smaller than for boreal streams in Wisconsin (USA; 0–2.8 µM; Crawford et al., 2017). Comparison suggests that our finding of high dissolved methane concentration is within the range of data on a global scale and does not exceed the spatial-temporal variation of those reported concentrations.

The total river flux estimated using calculation with transfer velocity in 2017 (9.4±3.5 mg CH_4 m^{-2} d^{-1}), of which 60% was sourced from the tributaries, was significantly higher than that in 2016 (2.6±1.1 mg CH_4 m^{-2} d^{-1}); daily emissions of river methane were 3.6 times higher in 2017 than in 2016 (Table 2). The large spatial variation of dissolved methane concentration, modeled in 2017, caused substantial differences in the flux estimation. The flux in the main-flow and tributaries in 2017 (flood) were 5.6±1.1 and 16.5±2.8 (mg CH_4 m^{-2} d^{-1}), respectively. In particular, the flux for tributaries in 2017 were higher than in previous research for Lena (0 mg CH_4 m^{-2} d^{-1} owing to measurement limit; Schneider et al., 2009), the Middle Yukon (6.2±2.1 mg CH_4 m^{-2} d^{-1}; Striegl et al., 2012) and the Kuparuk river in Alaska (5.8 mg CH_4 m^{-2} d^{-1}; Kling et al., 1992), but lower than the Lower Yukon (22±4.2 mg CH_4 m^{-2} d^{-1}; Striegl et al., 2012). Enhanced emissions at tributaries, covering 34% of the total river area, were evaluated to be 2.7×10^3 kg CH_4 per day, contributing 60% of riverine methane emissions. Previous studies have reported significant methane efflux in the growing season using the chamber method for the back swamp of a river margin (310–890 mg CH_4 m^{-2} d^{-1}), a polygonal sedge wetland (48–190 mg CH_4 m^{-2} d^{-1}) in the Indigirka lowland (van Huissteden el al 2005), and a polygonal wetland in the Lena delta (78–100 mg CH_4 m^{-2} d^{-1}; Sachs et al., 2010). Riverine methane emissions in this study are smaller than those from wetland soils on a daily scale. Nevertheless, riverine emissions and water-to-air transportation of dissolved methane should not be negligible while flood waters cover the land for more than a month, and flux through the wetland soil surface might be inhibited by water on a month-long time-scale. The estimation is also limited by the flux evaluation method applied from the constant transfer velocity, although the flux can be obtained from the difference in partial pressures between air and water of CH_4. Gas exchange rate is expected to be high in the turbulent conditions of water and atmosphere, in which the transport velocity (k_{CH4} in Eq 7) is high. Therefore, the river CH_4 flux may be linked to the hydrology which may be relating to the stream morphology of the rivers (Campeau et al., 2014), and these parameters are unknown in our study. There could still be underestimation of methane evasion under unusual water surface mixing conditions during flooding, and further research is needed to improve measurement of dissolved concentrations and the air–water surface exchange of methane for reliable estimation during extreme events.

5. Conclusions

Visible and near-infrared bands, recorded by high-resolution satellites, can be used for modeling the spatial variations of riverine methane concentrations. In this study, the best indicator for dissolved methane was the red band (636–673 nm), which responded to turbidity controlled by suspended sediment concentration enhanced under extreme flooding, and was negatively correlated with dissolved methane concentrations. The methods presented here for satellite observation of dissolved methane can provide a tool for in situ environmental monitoring in remote areas such as Siberia.

Acknowledgements

We would like to thank the Institute for Biological Problems of Cryolithozone, Siberian Branch of the Russian Academy of Sciences, the Allikhovsky Ulus Inspectorate of Nature Protection for fieldwork support. The Landsat 8 OLI data used in this study were provided by the United States Geological Survey.

Funding Sources

This work was supported by the JSPS KAKENHI [grant numbers JP21403011 and JP16J07265]; the Belmont Forum through the COPERA, C budget of Ecosystems, Cities and Villages on Permafrost in the eastern Russian Arctic.

References

Aufdenkampe, A. K., Mayorga, E., Raymond, P. A., Melack, J. M., Doney, S. C., Alin, S. R., Aalto, R. E., Yoo, K. 2011. Riverine coupling of biogeochemical cycles between land, oceans, and atmosphere. Frontiers in Ecology and the Environment, 9(1), 53-60.

Barbosa, P. M., Melack, J. M., Farjalla, V. F., Amaral, J. H. F., Scofield, V., Forsberg, B. R. 2016. Diffusive methane fluxes from Negro, Solimoes and Madeira rivers and fringing lakes in the Amazon basin. Limnology and Oceanography, 61, 221-237.

Billett, M. F., Harvey, F. H. 2013. Measurements of CO2 and CH4 evasion from UK peatland headwater streams. Biogeochemistry, 114(1-3), 165-181.

Brezonik, P. L., Olmanson, L. G., Finlay, J. C. & Bauer, M. E. 2015. Factors affecting the measurement of CDOM by remote sensing of optically complex inland waters. Remote Sensing of Environment, 157, 199-215.

Bussmann, I. 2013. Distribution of methane in the Lena Delta and Buor-Khaya Bay, Russia. Biogeosciences, 10(7), 4641-4652.

Campeau, A., Del Giorgio, P. A. 2014. Patterns in CH4 and CO2 concentrations across boreal rivers: Major drivers and implications for fluvial greenhouse emissions under climate change scenarios. Global Change Biology, 20(4), 1075-1088.

Campeau, A., Lapierre, J. F., Vachon, D. & del Giorgio, P. A. 2014. Regional contribution of

CO_2 and CH_4 fluxes from the fluvial network in a lowland boreal landscape of Quebec. Global Biogeochemical Cycles, 28(1), pp 57-69.

Crawford, J. T., Loken, L. C., West, W. E., Crary, B., Spawn, S. A., Gubbins, N., Jones, S. E., Striegl, R. G. & Stanley, E. H. 2017. Spatial heterogeneity of within-stream methane concentrations. Journal of Geophysical Research-Biogeosciences, 122(5)**,** 1036-1048.

Dyson, K. E., Billett, M. F., Dinsmore, K. J., Harvey, F., Thomson, A. M., Piirainen, S. Kortelainen, P. 2011. Release of aquatic carbon from two peatland catchments in E. Finland during the spring snowmelt period. Biogeochemistry, 103(1-3), 125-142.

Fernandez, J. E., Peeters, F., Hofmann, H. 2016. On the methane paradox: Transport from shallow water zones rather than in situ methanogenesis is the major source of CH_4 in the open surface water of lakes. Journal of Geophysical Research-Biogeosciences, 121(10), 2717-2726.

Frey, K. E., McClelland, J. W. 2009. Impacts of permafrost degradation on arctic river biogeochemistry. Hydrological Processes, 23(1), 169-182.

Huh, Y., Tsoi, M. Y., Zaitsev, A., Edmond, J. M. 1998. The fluvial geochemistry of the rivers of eastern Siberia: I. Tributaries of the Lena River draining the sedimentary platform of the Siberian Craton. Geochimica Et Cosmochimica Acta, 62(10), 1657-1676.

Iwahana, G., Takano, S., Petrov, R. E., Tei, S., Shingubara, R., Maximov, T. C., Fedorov, A. N., Desyatkin, A. R., Nikolaev, A. N., Desyatkin, R. V., Sugimoto, A. 2014. Geocryological characteristics of the upper permafrost in a tundra-forest transition of the Indigirka River Valley, Russia. Polar Science, 8(2), 96-113.

James, A. L. Roulet, N. T. 2006. Investigating the applicability of end-member mixing analysis (EMMA) across scale: A study of eight small, nested catchments in a temperate forested watershed. Water Resources Research, 42(8), 17.

Karlsson, J., Giesler, R., Persson, J., Lundin, E. 2013. High emission of carbon dioxide and methane during ice thaw in high latitude lakes. Geophysical Research Letters, 40(6), 1123-1127.

Langer, M., Westermann, S., Anthony, K. W., Wischnewski, K., Boike, J. 2015. Frozen ponds: production and storage of methane during the Arctic winter in a lowland tundra landscape in northern Siberia, Lena River delta. Biogeosciences, 12(4), 977-990.

Liang, M. C., Sugimoto, A., Tei, S., Bragin, I. V., Takano, S., Morozumi, T., Shingubara, R., Maximov, T. C., Kiyashko, S. I., Velivetskaya, T. A., Ignatiev, A. V. 2014. Importance of soil moisture and N availability to larch growth and distribution in the Arctic taiga-tundra boundary ecosystem, northeastern Siberia. Polar Science, 8(4), 327-341.

McFeeters, S. K. 1996. The use of the normalized difference water index (NDWI) in the delineation of open water features. International Journal of Remote Sensing, 17(7), 1425-1432.

Mertes, L. A. K., Smith, M. O., Adams, J. B. 1993. Estimating suspended sediment concentrations in surface waters of the Amazon river wetlands from Landsat images. Remote Sensing of Environment, 43(3), 281-301.

Morishita, T., Matsuura, Y., Kajimoto, T., Osawa, A., Zyryanova, O. A. & Prokushkin, A. S. 2014. CH4 and N2O dynamics of a Larix gmelinii forest in a continuous permafrost region of central Siberia during the growing season. Polar Science, 8(2), pp 156-165.

Morozumi, T., Shingubara, R., Fan, R., Takano, S., Tei, S., Maximov, T. C., Kobayashi, H., Suzuki, R. & Sugimoto, A. 2016. High resolution vegetation mapping for upscaling of local CH4 emission in Taiga-Tundra boundary, eastern Siberia. proceeding of International Symposium on Remote Sensing, 2016 Korea.

Morozumi, T., Shingubara, R., Tei, S., Fan, R., Takano, S., Kobayashi, H., Suzuki, R., Maximov, T. C. & Sugimoto, A. 2017. Methane dynamics in river lowland, north eastern Siberia: short term influence of extreme flooding on river water dissolved methane in 2017 summer. The 63rd Autumn Conference of the Remote Sensing Society of Japan. Japan.

Murase, J., Sakai, Y., Sugimoto, A., Okubo, K., Sakamoto, M. 2003. Sources of dissolved methane in Lake Biwa. Limnology, 4(2), 91-99.

Neal, C., Jarvie, H. P., Williams, R., Love, A., Neal, M., Wickham, H., Harman, S., Armstrong, L. 2010. Declines in phosphorus concentration in the upper River Thames (UK): Links to sewage effluent cleanup and extended end-member mixing analysis. Science of the Total Environment, 408(6), 1315-1330.

R Core Team. 2013. R foundation for statistical computing. Vienna, Austria. ISBN 3-900051-07-0, URL http://www.R-project.org.

Rokni, K., Ahmad, A., Selamat, A., Hazini, S. 2014. Water Feature Extraction and Change Detection Using Multitemporal Landsat Imagery. Remote Sensing, 6(5), 4173-4189.

Sawakuchi, H. O., Bastviken, D., Sawakuchi, A. O., Krusche, A. V., Ballester, M. V. R., Richey, J. E. 2014. Methane emissions from Amazonian Rivers and their contribution to the global methane budget. Global Change Biology, 20(9), 2829-2840.

Sawamoto, T., Takakai, F., Desyatkin, A. R., Desyatokin, R. V. & Hatano, R. 2006. Dissolved N2O and CH4 in seepage and stream water in Yakutsk, R. Hatano, G. Guggenberger (Eds.), Symptom of Environmental Change in Siberian Permafrost Region, Sapporo, Japan: Hokkaido University Press.

Semiletov, I. P., Pipko, II, Shakhova, N. E., Dudarev, O. V., Pugach, S. P., Charkin, A. N., McRoy, C. P., Kosmach, D., Gustafsson, O. 2011. Carbon transport by the Lena River from its headwaters to the Arctic Ocean, with emphasis on fluvial input of terrestrial particulate organic carbon vs. carbon transport by coastal erosion. Biogeosciences, 8(9), 2407-2426.

Shakhova, N. E., Semiletov, I. P., Bel'cheva, N. N. 2007. The great Siberian rivers as a source of methane on the Russian Arctic shelf. Doklady Earth Sciences, 415(5), 734-736.Shingubara, R., Sugimoto, A., Murase, J., Tei, S., Takano, S., Morozumi, T., Liang, M., Iwahana, G. & Maximov, T. C. 2016. Multi-year response of CH_4 efflux to wetting at Indigirka Lowland in Northeastern Siberia. Japan Geoscience Union Meeting. Chiba, Japan.

Stanley, E. H., Casson, N. J., Christel, S. T., Crawford, J. T., Loken, L. C., Oliver, S. K. 2016. The ecology of methane in streams and rivers: patterns, controls, and global significance. Ecological Monographs, 86(2), 146-171.

Street, L. E., Dean, J. F., Billett, M. F., Baxter, R., Dinsmore, K. J., Lessels, J. S., Subke, J. A., Tetzlaff, D., Wookey, P. A. 2016. Redox dynamics in the active layer of an Arctic headwater catchment; examining the potential for transfer of dissolved methane from soils to stream water. Journal of Geophysical Research-Biogeosciences, 121(11), 2776-2792.

Striegl, R. G., Dornblaser, M. M., McDonald, C. P., Rover, J. R., Stets, E. G. 2012. Carbon dioxide and methane emissions from the Yukon River system. Global Biogeochemical Cycles, 26, GB0E05, doi:10.1029/2012GB004306.

Suzuki, K., Matsuo, K., Hiyama, T. 2016. Satellite gravimetry-based analysis of terrestrial water storage and its relationship with run-off from the Lena River in eastern Siberia. International Journal of Remote Sensing, 37(10), 2198-2210.

van Huissteden, J., Maximov, T. C. & Dolman, A. J. 2005. High methane flux from an arctic floodplain (Indigirka lowlands, eastern Siberia). Journal of Geophysical Research-Biogeosciences, 110(G2).

Volpe, V., Silvestri, S., Marani, M. 2011. Remote sensing retrieval of suspended sediment concentration in shallow waters. Remote Sensing of Environment, 115(1), 44-54.

Wanninkhof, R. 1992. Relationship between wind-speed and gas-exchange over the ocean. Journal of Geophysical Research-Oceans, 97(C5), 7373-7382.

Ward, D. P., Hamilton, S. K., Jardine, T. D., Pettit, N. E., Tews, E. K., Olley, J. M., Bunn, S. E. 2013. Assessing the seasonal dynamics of inundation, turbidity, and aquatic vegetation in the Australian wet dry tropics using optical remote sensing. Ecohydrology, 6(2), 312-323.

Xiao, Q. T., Zhang, M., Hu, Z. H., Gao, Y. Q., Hu, C., Liu, C., Liu, S. D., Zhang, Z., Zhao, J. Y., Xiao, W., Lee, X. 2017. Spatial variations of methane emission in a large shallow eutrophic lake in subtropical climate. Journal of Geophysical Research-Biogeosciences, 122(7), 1597-1614.

Yabuki, H., Park, H., Kawamoto, H., Suzuki, R., Razuvaev, V.N., Bulygina, O.N., Ohata, T., 2011. Baseline Meteorological Data in Siberia (BMDS) Version 5.0. RIGC, JAMSTEC, Yokosuka, Japan distributed by CrDAP, Digital media.

Yamamoto, S., Alcauskas, J. B., Crozier, T. E. 1976. Solubility of methane in distilled water and seawater. Journal of Chemical & Engineering Data, 21(1), 78-80.

Table and Figure captions

Table 1. Landsat 8 OLI satellite images used in flood detection.

Acquisition Date (dd-mm-yy)	Path/Row[1]	Surface Condition[2]	Solar angle zenith (deg)	Azimuth (deg)[3]
29-6-16	115/10	dry	47.75	175.95
29-7-16	117/10	dry	52.3	175.25
07-8-16	116/10	dry	54.63	175.55
11-7-17	114/10	flood	48.88	175.37
11-7-17	114/11	flood	47.63	173.01
27-7-17	114/10	after flood	51.78	175.18
27-7-17	114/11	after flood	50.54	172.89

[1]Location identifier using the global notation system for Landsat data.

[2]Condition of the land surface (whether flooded or not).

[3]Horizontal angle relative to north from the observer.

Table 2. Predicted dissolved methane concentration [CH_4], saturation ratio of dissolved methane in equilibrium, flux as average and SD, total methane emission in the study area per day, and contribution of methane flux from the main channel and tributaries.

Year	Category	Area[*1] (km^2)	CH_4 concentration (μM)[*2]	saturation ratio[*3]	Flux ($mgCH_4$ m^{-2} d^{-1})[*4]	Daily CH_4 emission ($kgCH_4$ d^{-1})	Regional contribution %
2017	All	483.3	0.47±0.17	242	9.4±3.5	4544	
	Main channel	319.5	0.36±0.07	187	5.6±1.1	1839	40.5
	Tributary	163.9	0.68±0.12	351	16.5±2.8	2705	59.5
2016[*5]	All	483.3	0.17±0.04[*5]	86	2.6±1.1	1257[*6]	

[1]Study area covers a 250 × 350 km region in the Indigirka River lowlands.

[2]Dissolved methane concentration predicted by the empirical model.

[3]Saturation ratio of dissolved methane against solubility of dissolved methane in equilibrium.

[4]Average methane flux from water surface to the atmosphere estimated from predicted dissolved methane concentration.

[5]Average dissolved methane in 2016 among the main-channel and tributaries using observed values.

[6]Total methane emission calculated from observed mean flux in 2016 multiplied by total river area.

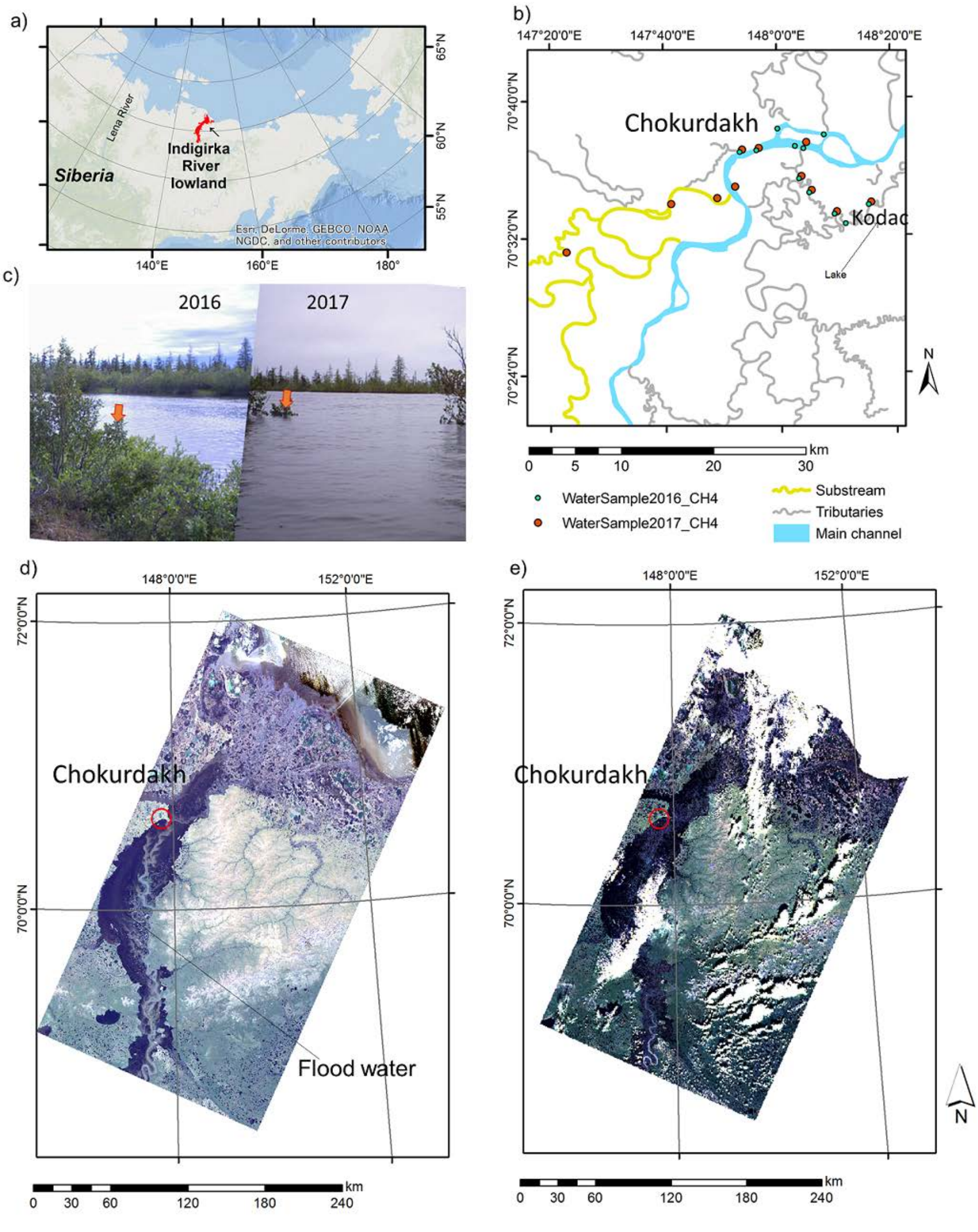

Figure 1. Study sites and sampling locations for a typical year in 2016 and an extreme flooding event in 2017: (a) Observation area in the region; (b) Sampling sites for dissolved methane near

Chokurdakh and Kodac; (c) Photographs recorded along a tributary near Kodac during the summers of 2016 and 2017; (d) Landsat 8 true color image during the peak of flooding on 11 July 2017; (e) Landsat 8 true color image during flood decline on 27 July 2017 (6.0×10^4 km^2). Red circle indicates location of the town of Chokurdakh. White blank on the image is a cloudy area (1.3×10^4 km^2) that was excluded from the analysis.

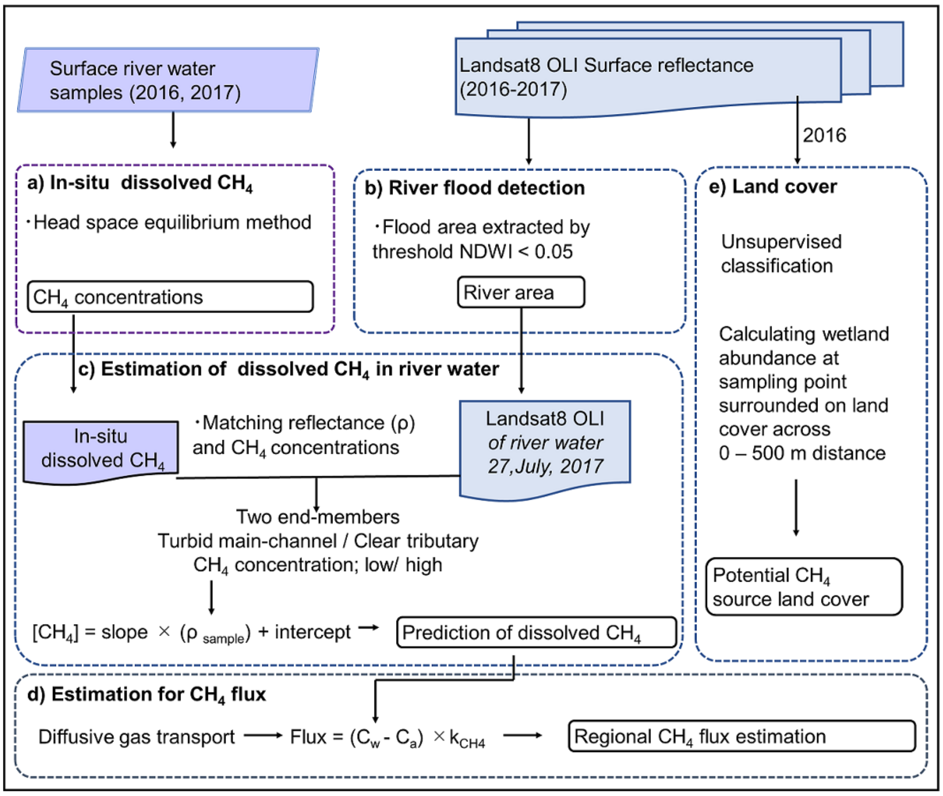

Figure 2. Flow chart for data processing. (a) In-situ dissolved methane in river water; (b) river flooding detection with Landsat 8 on 11 and 27 July 2017; (c) modeling for dissolved methane with in-situ methane concentrations and reflectance; (d) regional methane emissions calculated using a diffusive transport model; (e) land cover identified using unsupervised classification to detect potential methane sources. Abbreviations note reflectance on Landsat8 (ρ), concentration

of dissolved methane ([CH_4]), and slope and aspect of regression to predict dissolved methane. Abbreviations for flux calculation are concentration of methane in water (C_w)and air (C_a), and the gas transfer velocity of methane between water and air (k_{CH4}).

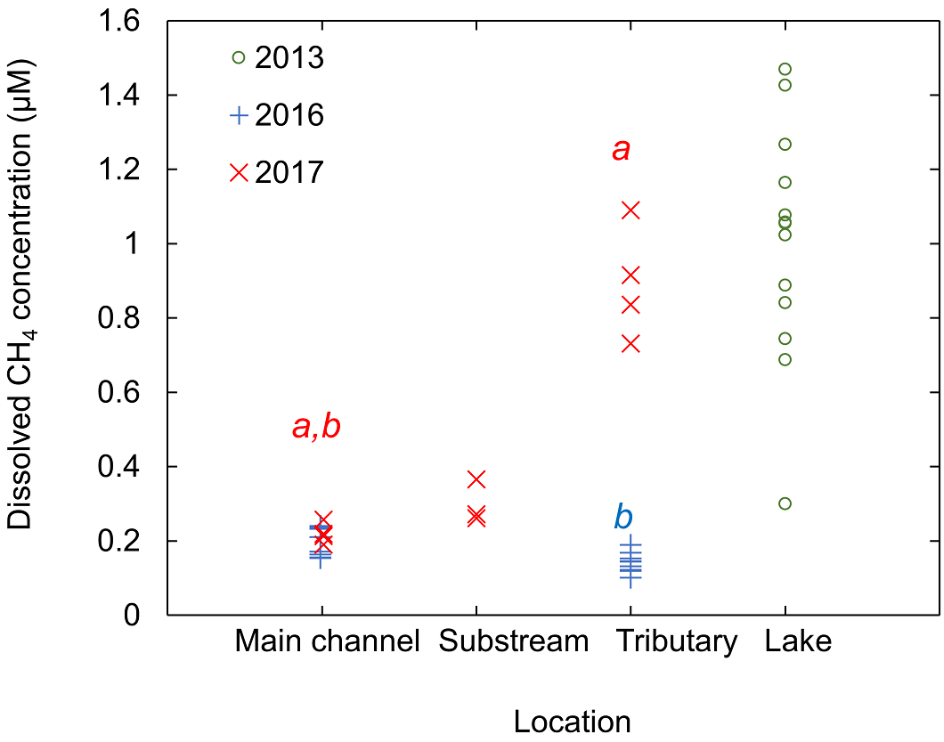

Figure 3. Dissolved methane concentrations (μM) in the main channel, substream, tributaries, and lake observed in July 2013, 2016, and 2017. Significant differences between the main channel and tributary in 2017 are marked as *a* ($P < 0.005$), and in 2016 with as *b* ($P < 0.005$).

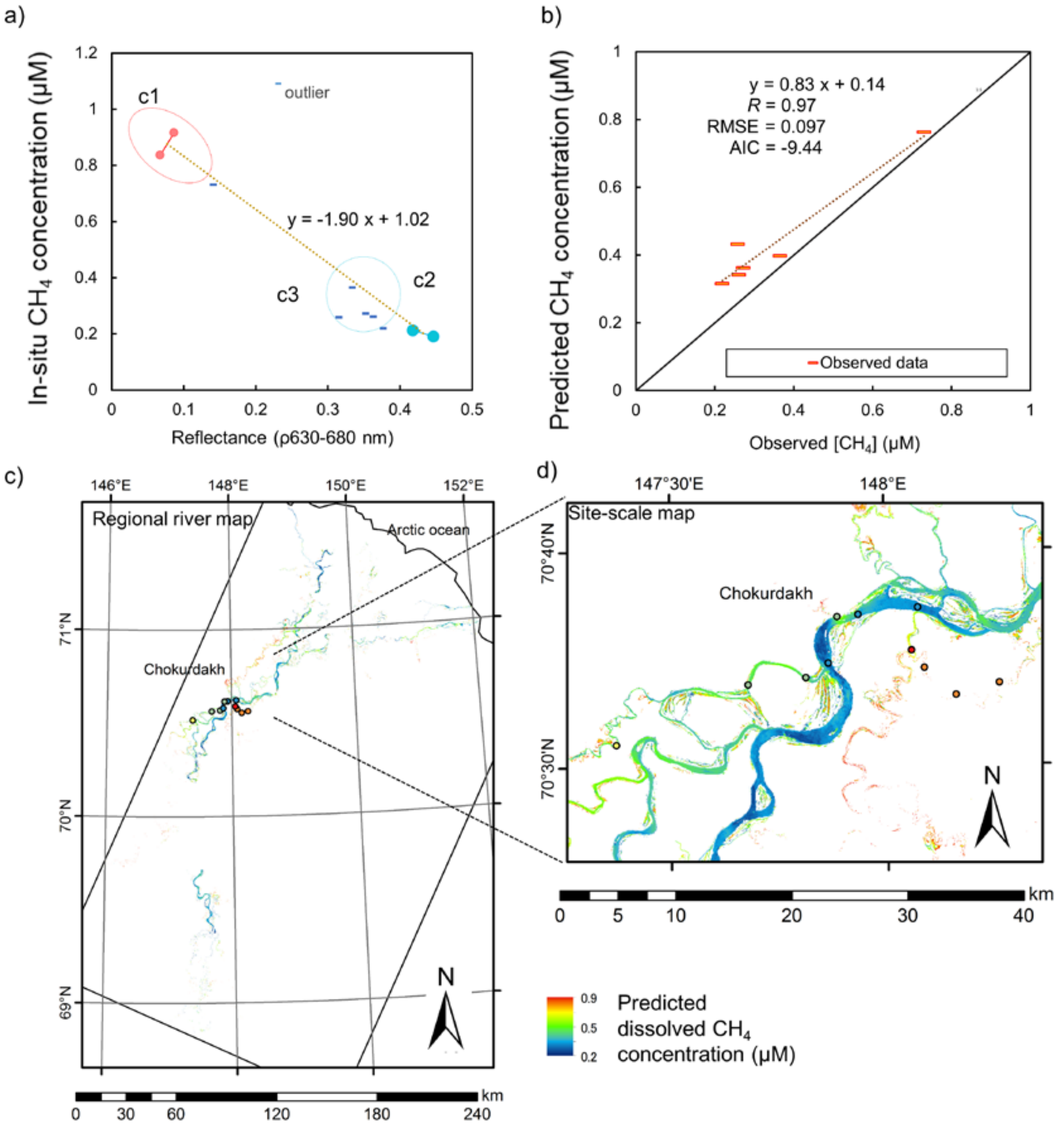

Figure 4. Empirical endmember mixing model for dissolved methane concentrations (μM) and satellite reflectance from the red band (630–680 nm). Surface reflectance values were expressed in a scale of 0-10 ($\times 10^{-1}$). (a) Relationship between reflectance from the red band (636–673 nm) and in-situ dissolved methane, with notations for endmembers of higher concentration with low reflectance (c1), lower concentrations with high reflectance (c2), and intermediate (c3); (b) In-situ dissolved methane and predicted methane concentration with an empirical endmember

mixing model from satellite reflectance from the red band (636–673 nm) with the 1:1 line, correlation coefficient (*R*), root mean square error (RMSE), and Akaike information criteria (AIC); (c) Distribution map of river dissolved methane concentrations drawn by an empirical endmember mixing model with satellite reflectance from the red band (636–673 nm) in the lower Indigirka River region. (d) Enlarged view around the sampling area; cloud, lake, and land areas were excluded from the analysis.

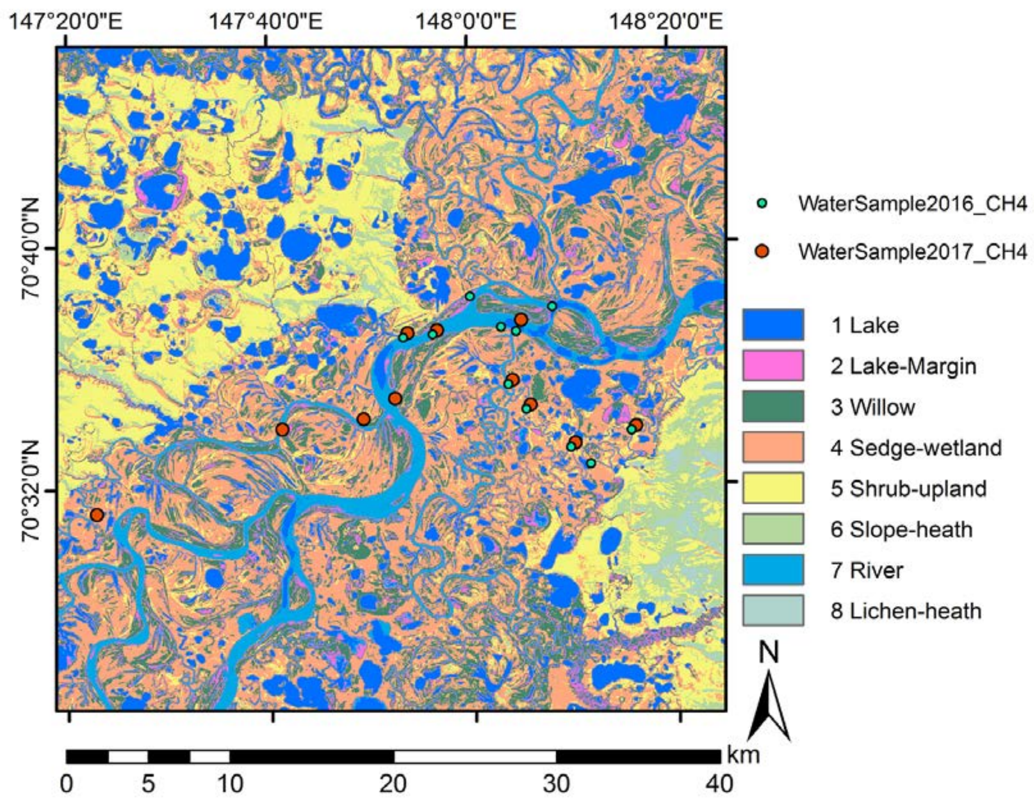

Figure 5. Land cover properties classified from a Landsat 8 image on 7 August 2016.

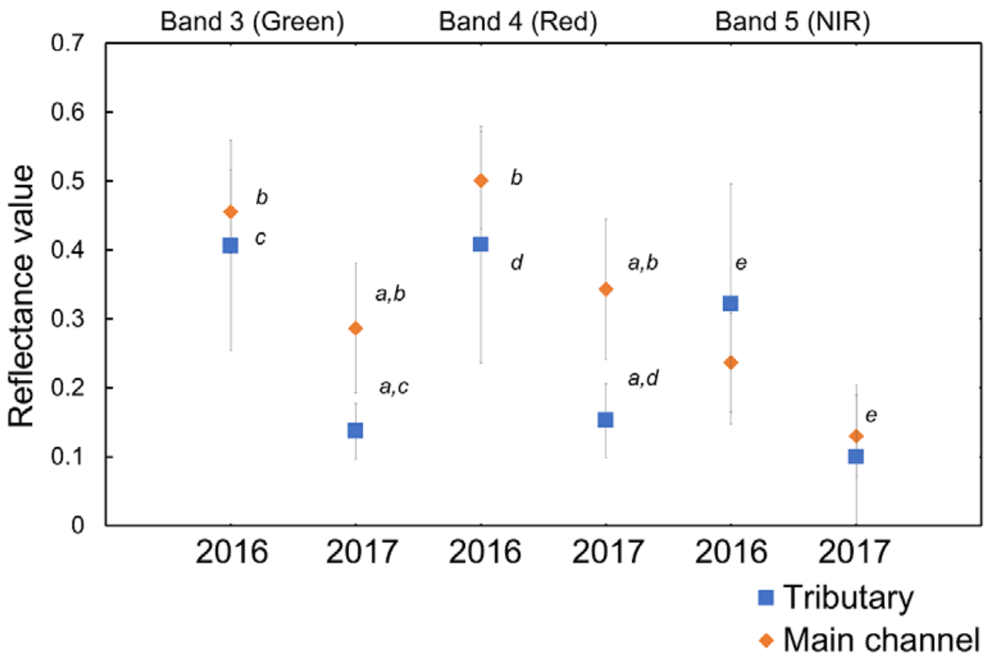

Figure S1. Surface reflectance of the tributary and main channel in June-August 2016 (non-flood) and 2017 (extreme flood), shown as average ±SD; with a scale factor of 0-10 (× 10^{-1}). Reflectance values were collected in the water sampling site at four points in tributary and seven points along the main-flow; for each, Band 3, Band 4, and Band 5 reflectance was compared. Significant differences between tributary and main-flow in 2017 is shown with *a* (P < 0.001). Differences between 2016 and 2017 for the main-flow are shown with *b* (P < 0.001), and difference between 2016 and 2017 for the tributaries is shown with *c* (P < 0.001), *d* (P < 0.005) and e (P < 0.01).

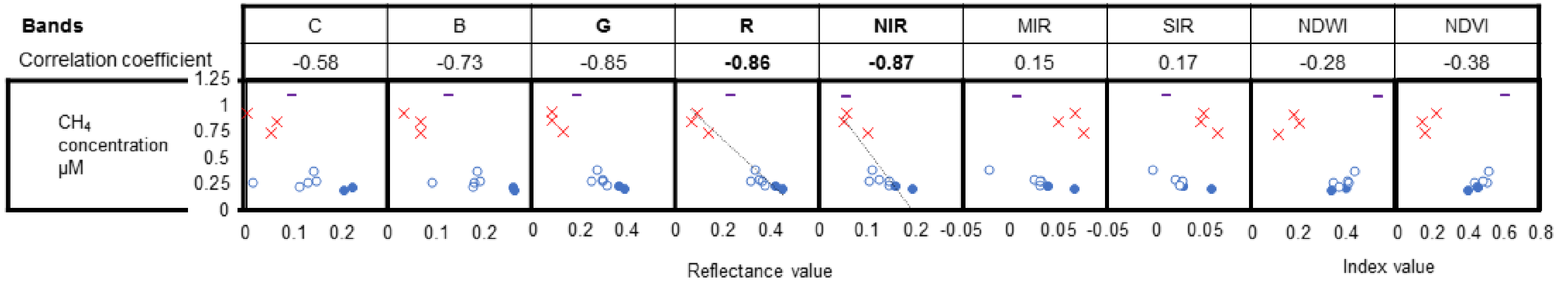

Figure S2. Multivariate correlation analysis on satellite surface reflectance (coastal, blue, green red near-infrared shortwave-infrared1, shortwave-infrared2 band) and water indices against dissolved CH_4 concentration. Each legend indicates the different clusters of red x-marks (c1), blue filled circles (c2), blue blank circles (c3), and purple bars (c4-outlier).

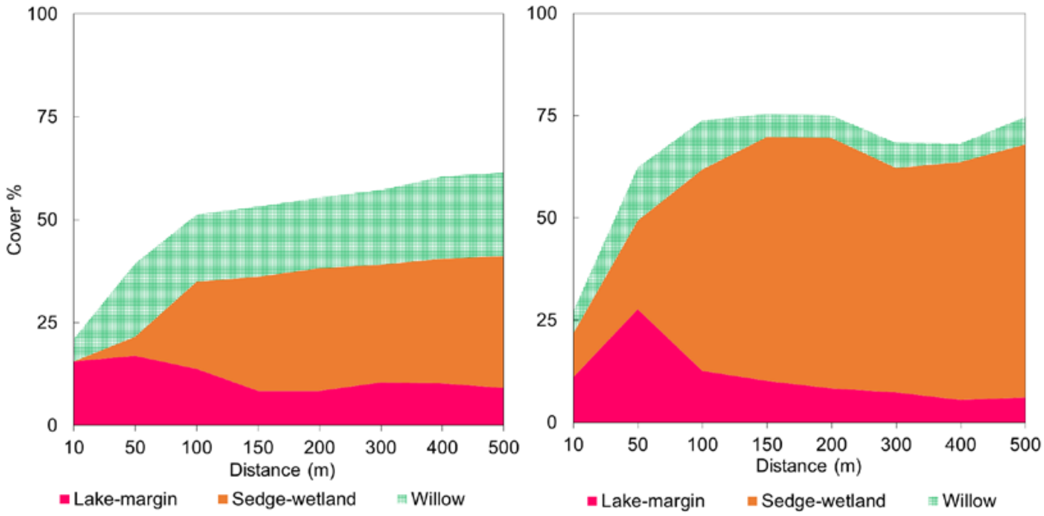

Figure S3. Land cover properties of surrounding areas (0–500m distances from each sampling point). Tributary sampling points were adjacent to the lake-margin and sedge-wetland, implying potential CH_4 sources, whereas the main-flow was adjacent to willow bush, implying no-source.